Nuclear Instruments and Methods in Physics Research A 377 (1996) 375–380

ELSEVIER

NUCLEAR INSTRUMENTS & METHODS IN PHYSICS RESEARCH Section A

A new silicon drift detector with reduced lateral diffusion

A. Castoldi[a,*], P. Rehak[b], P. Holl[c]

[a]*Universita' degli Studi, Dipartimento di Fisica, Via Celoria 16, 20133 Milano, Italy*
[b]*Brookhaven National Laboratory Upton, NY 11973, USA*
[c]*MPI Halbleiterlabor, Paul-Gerhardt-Allee 42, D-81245 München, Germany*

Abstract

We present a method to reduce the effect of diffusion in the direction transverse to the drift in silicon drift detectors. This is achieved by creating regions of deep p-implant parallel to the drift direction that act as rigid guidelines during the drift of the charge cloud generated by a radiation interaction. The influence of the deep implanted acceptors on the lateral confining field is discussed. A prototype has been designed, fabricated and tested. First experimental results are reported which demonstrate the achieved reduction of the lateral width of the electron cloud with respect to free broadening.

1. Introduction

In the case of the "classical" multi-anode Silicon Drift Detector (SDD) [1,2], the electrons generated in the detector volume by ionising radiation drift at constant velocity in the center plane of the detector towards an array of anodes. During the drift, diffusion and electrostatic repulsion broaden the electron cloud in the directions parallel to the surface of the detector [3]. The charge generated by a radiation interaction may therefore be shared by contiguous anodes. This sharing can be exploited to measure the coordinate transverse to the drift direction (lateral coordinate) because it allows a resolution better than the pitch of the anodes. However the transverse width of the electrons arriving at the anodes may be too wide when arriving to the anodes after drifting and diffusing for several microseconds. To achieve the best possible resolution in the transverse direction the signal electrons should diffuse only to the correct width at the beginning of the drift. Once the electrons are diffused sufficiently, the process of diffusion should stop. The position is then obtained from the charge sharing of signals on two anodes with an optimal precision and independently of the drift distance. Lateral diffusion also limits the maximum number of allowed interactions per unit area. In fact each anode does not only collect from the active area faced to it, as the collection areas of several contiguous anodes overlap. The pulse rate seen at each anode is therefore greater than the ideal minimum value (total event rate)/(no. of anodes) and depends on the electron diffusion. Also for these rate considerations it would be desirable to reduce the lateral diffusion of the electron cloud in order to collect the full signal charge at very few (1–2) anodes, independently of the position of interaction.

We here present a new drift detector design aimed to prevent the lateral diffusion of the electron cloud and the first experimental results. The drift detector project was carried through as a parasitic test during the production of fully depleted CCDs for the XMM satellite mission [4]. The prototype of the drift detector presented in this paper conformed to the starting epitaxial silicon material and to all production steps of the CCD production.

2. Design and simulation

Fig. 1 shows a schematic view of the new detector design. It is characterized by an array of deep p-implants ("channel-stops") parallel to the drift direction of an n-bulk drift detector. This channel-stop mechanism is similar with the one previously developed by Strüder et al. [5,6] for the fully depleted pn-CCDs. There in addition to the deep p structures a deep n-implant is introduced to guide the electrons during the clocked transfer to the read-out anodes.

Differently from the "classical" SDD, a much lower negative potential is applied to the anode side of the detector than on the opposite side of the wafer (back side). The trajectory of the charge cloud is thus displaced close to the implanted surface (anode side), where the small potential barrier generated by the ionised acceptors of the deep implants is able to confine the electrons within two neighbouring channel-stops during the drift. A thin epitaxial layer, having lower resistivity than the substrate, prevents thermal injection of holes from the p+ strips on the deep implanted side to the p+ strips on the back side, and forms a guiding layer for the electrons.

* Corresponding author.

PII S0168-9002(96)00019-8

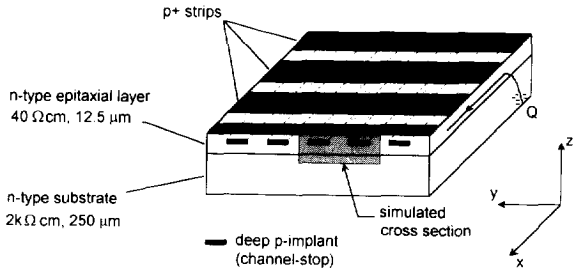

Fig. 1. Perspective view (not to scale) of the drift region of the new drift detector with deep "channel-stop" implants. Resistivity and thickness of the substrate and of the epitaxial layer are shown.

Diffusion and repulsion can spread the electron cloud only during the initial motion of electrons, before reaching the minimum of the potential energy near the deep implanted surface. The width of the cloud arriving in the potential minimum depends on the depletion field and on the starting distribution of the generated electrons. For a given type of radiation, however, the width of the electron cloud that reaches the potential minimum will be independent of the (x, y) position of interaction on the detector surface. For an optimal energy resolution this initial width should be minimised in order to avoid charge sharing. Some charge sharing between two drift channels instead always occurs when the initial electron spread at least equals the width of the drift channel. This initial division of the signal charge is then frozen during the drift. The measurement of the charge collected at two individual anodes allows to determine the lateral coordinate of the centroid (y) with a resolution much better than the anode pitch. Most of the methods give the spatial position with an error σ_y which depends on the anode pitch as:

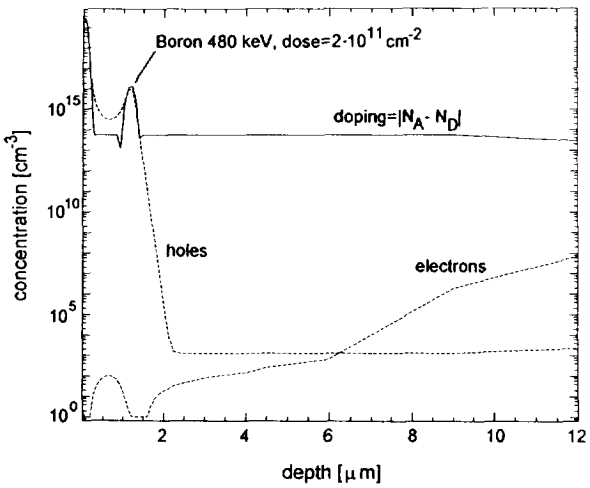

Fig. 2. 1-D profile of the net doping and of the electron and hole concentrations in the epitaxial layer of the detector across the shallow and deep p-implant.

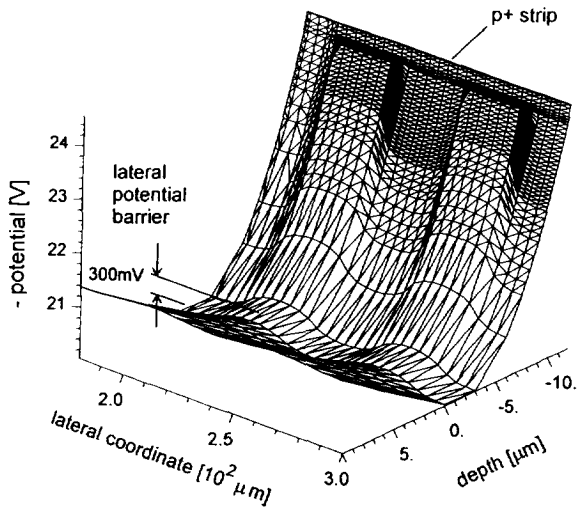

Fig. 3. Potential energy for electrons (negative potential) in the detector cross section perpendicular to the drift indicated in Fig. 1. The effect of two regions of deep implants is visible.

$$\frac{\sigma_y}{P_y} = \frac{\mathrm{ENC}}{Q}, \tag{1}$$

where P_y is the anode pitch (corresponding to the pitch of the deep p-implants), ENC is the equivalent noise charge relative to one channel and Q is the signal charge.

To investigate the effect of the implanted ionised impurities on the potential near the surface, we used the two-dimensional device simulator HFIELDS, which solves the system of the Poisson equation and continuity equations for both carriers in semiconductors [7]. Fig. 2 shows the simulated doping profile in the epitaxial layer and the calculated carrier densities. The channel-stop implant (boron, 480 keV, dose $= 2 \times 10^{11}$ cm^{-2}) is only partially depleted (about 40% of the implanted dose is depleted) and is in electric contact with the shallow p+ implant due to a high density layer of holes. Fig. 3 shows the calculated potential energy for electrons (negative potential) in a detector cross-section perpendicular to the drift direction (the simulated region is dashed in Fig. 1). In the minimum of the potential energy, located at the interface between substrate and epitaxial layer ($z = 0$), a lateral potential barrier $\Delta V_b = 300$ mV for electron confinement is obtained. In Fig. 4 the one-dimensional cut of the potential through the shallow and deep implants shows that the deep p-implant is approximately at the same potential of the p+ strip on the surface. The effect of the channel-stop implant can be therefore interpreted as a modulation of the thickness of the epitaxial layer with an amplitude equal to the projected range of the deep implant. An equivalent potential perturbation ΔV_s on the surface can be defined and can be estimated by one dimensional calculation:

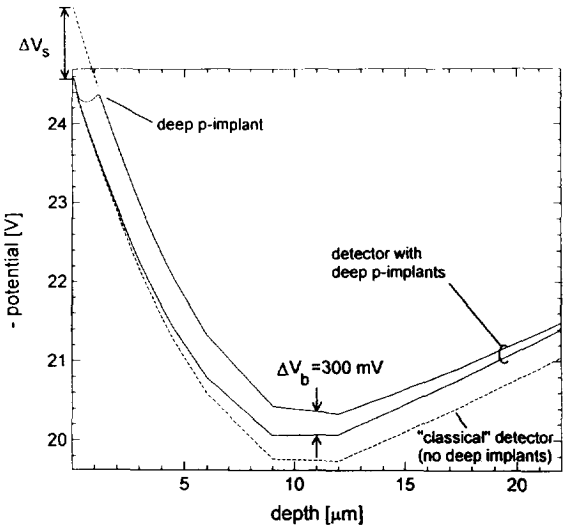

Fig. 4. 1-D profile of the potential energy for electrons (negative potential) for a "classical" drift detector without deep implants (dashed line) and for the new drift detector prototype (solid lines). The upper solid line is the 1-D cut crossing the shallow implant and the centre of the "channel-stop" implant. The lower solid line crosses only the shallow implant in the middle of the drift channel.

$$\Delta V_s \cong \left(\frac{qN_{epi}}{\varepsilon} z_{epi}\right) z_{dp}, \quad (z_{dp} \ll z_{epi}), \tag{2}$$

where N_{epi}, z_{epi} are respectively doping and thickness of the epitaxial layer and z_{dp} is the projected range of the deep implant. Eq. (2) shows that the choice of the epitaxial layer is essential to achieve a significant lateral barrier. Changes of the implanted dose up to $4 \times 10^{12}\,\mathrm{cm}^{-2}$ produce negligible change in the lateral confining potential.

A lateral potential barrier greater than a few thermal voltages succeeds in confining only a small number of electrons, when electrostatic repulsion is negligible with respect to thermal diffusion. For an increasing number of electrons a threshold value is expected when repulsion overcomes the confining field. An estimate of the threshold is obtained by assigning to each electron, in addition to its thermal energy, a term accounting for the average repulsion energy. The average electrostatic energy per electron qV_{rep} for N electrons uniformly distributed inside a sphere of radius R is expressed by:

$$V_{rep} = \frac{q}{4\pi\varepsilon} \frac{3}{5} \frac{N}{R}, \tag{3}$$

which shows the dependence on the total number of electrons and the size of the confinement. Assuming that $V_{rep} \leq 1/3\,\Delta V_b$ for successful confinement and solving Eq. (3) for N, an approximate threshold of 4×10^4 electrons is obtained for $\Delta V_b = 300$ mV and $R = P_y/2 = 30$ μm.

3. Experimental results

The designed drift detector has been fabricated, mounted and tested. Fig. 5 shows the metallization mask of the active area and guard area of the detector prototype (anode side). The center strip is biased at the highest negative potential therefore electrons can drift either towards the upper or lower group of anodes. The maximal drift length is about 4.5 mm. The strip pitch on the anode side, closer to the electron trajectory, is made finer ($P_x = 40$ μm) than the one on the opposite side. An array of about 140 anodes with a pitch $P_y = 60$ μm is available to sample the charge cloud. Front-end electronics is integrated on the detector wafer close to each anode. The implanted channel-stops (boron, 480 eV, dose $2 \times 10^{11}\,\mathrm{cm}^{-2}$) have been realised only on the right half of the active area of the detector, while in the left half the cloud can broaden freely like in a classical drift detector. This allows to investigate in the same detector sample the diffusive properties of the electron cloud in presence or absence of a lateral confining field. In order to avoid a possible reduction of the threshold for the onset of a punch-through current between the shallow p+ strips, the regions of deep implant are interrupted in correspondence to the oxide gaps between the p+ strips.

A pulsed semiconductor laser (904 nm) with a pulse duration of the order of a few nanoseconds was focused on the deep implanted side of the detector to generate the signal electrons. The laser intensity was adjusted to generate $Q = 0.8$–1.6×10^4 electrons, well below the threshold for high charge effects.

The detector was operated at a drift field of 490 V/cm and the trajectory of the electron cloud was positioned at $\Delta z \cong 12$ μm from the surface, practically at the interface between epitaxial layer and substrate. The electron drift time as a function of the drift distance has been measured in two detector samples up to a total drift time of 1 and 3 μs respectively. Full collection of the injected charge is observed in both cases up to the maximal drift distance (4.5 mm). The average electron velocity in the drifting region shows a reduction of 10% in the first and of 50% in the second sample with respect to the unperturbed value due to the non-linearity of the surface potential [8]. Such perturbation can be reduced with higher values of the ratio $\Delta z/P_x$. In order to avoid instabilities of the electron velocity, the humidity of the detector environment, which affects the surface potential [8,9], has been stabilised during the measurements.

Measurements of the lateral diffusion of the electron cloud are obtained by sampling the projected electron density along the lateral coordinate. A sample interval smaller than the anode pitch is achieved by measuring the charge collected at the same anode for different lateral displacements of the laser spot. Charge collection at two individual anodes, corresponding to two adjacent drift channels, is shown in Fig. 6 as a function of the lateral

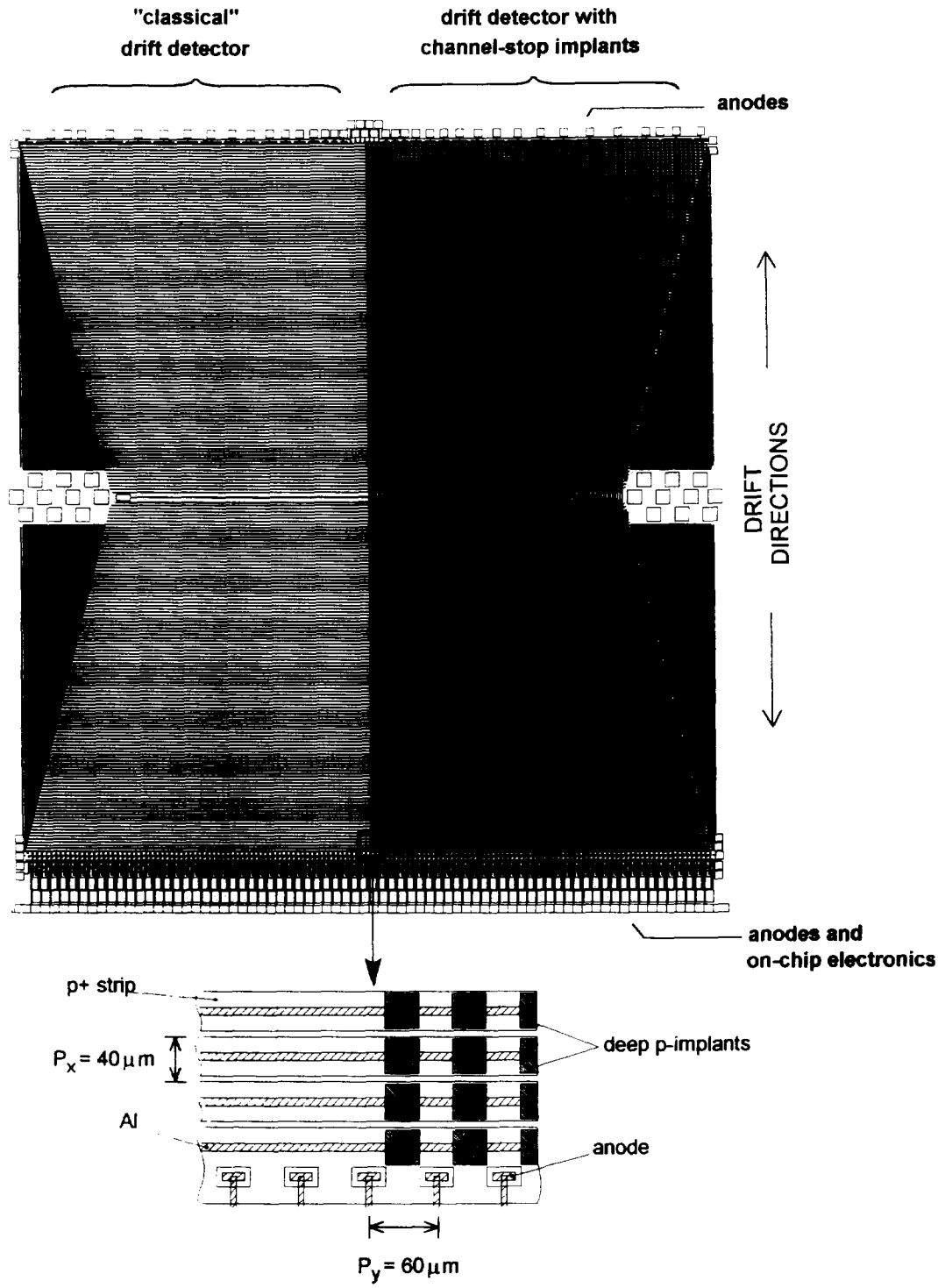

Fig. 5. Metallization mask of the SDC used in the experiment (anode side). The active area is about $9 \times 8\ mm^2$. Details of the electrode layout and of the "channel-stop" deep implants near the collecting anodes are also reported.

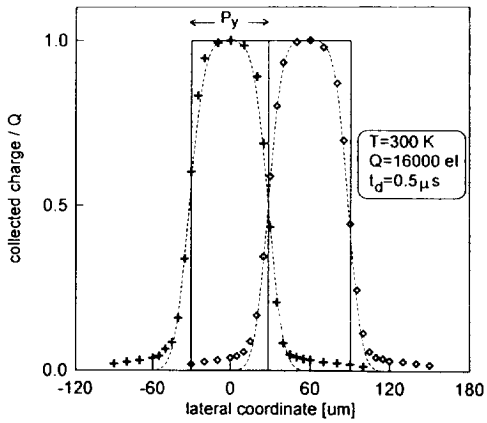

Fig. 6. Charge collected at two adjacent drift channels as a function of the lateral position of the injection point. The dashed lines are least-squares fits of the experimental points obtained by convolving a Gaussian (intensity of the laser pulse) with the rectangular weighting function of one anode, shown in solid line.

position of injection. All the injected charge remains confined within the starting drift channel throughout the drift. Charge sharing of the injected charge occurs near the edges of the channels because of the finite size of the laser spot. De-convolution of the experimental data from the rectangular weighting function of the anode, gives an estimate of the spot size (~15 μm) in agreement with independent optical measurements. In Figs. 7a and 7b we compare the electron broadening in presence and absence of the channel-stop implants. The reduction of the lateral width of the cloud when the channel-stop implants are present is already evident after a drift time of 0.5 μs (Fig. 7a). For higher drift times the electron cloud is still confined within one drift channel while free diffusion has already spread the electrons over several anodes (Fig. 7b). These results confirm that each anode collects from the active area directly faced to it without sharing the signal charge with adjacent anodes and demonstrate the effectiveness of the channel-stop implants in the reduction of the lateral diffusion of electrons.

The relevant parameters (centroid, total charge and rms width) of the projected electron density in the free diffusion case can be obtained by fitting the experimental points with the convolution of a Gaussian and the rectangular weighting function of the anode. The good agreement of the least-square fits with the experimental points confirms that the projected electron density along the lateral coordinate has Gaussian shape at the injected charge level, as expected from the well known solution of the continuity equation for pure diffusion.

A set of similar measurements has been done for different drift times, by varying the drift field and the drift distance up to $t_d = 3$ μs. The lateral rms widths of the projected electron density in case of free and reduced broadening are plotted in Fig. 8 as a function of the drift

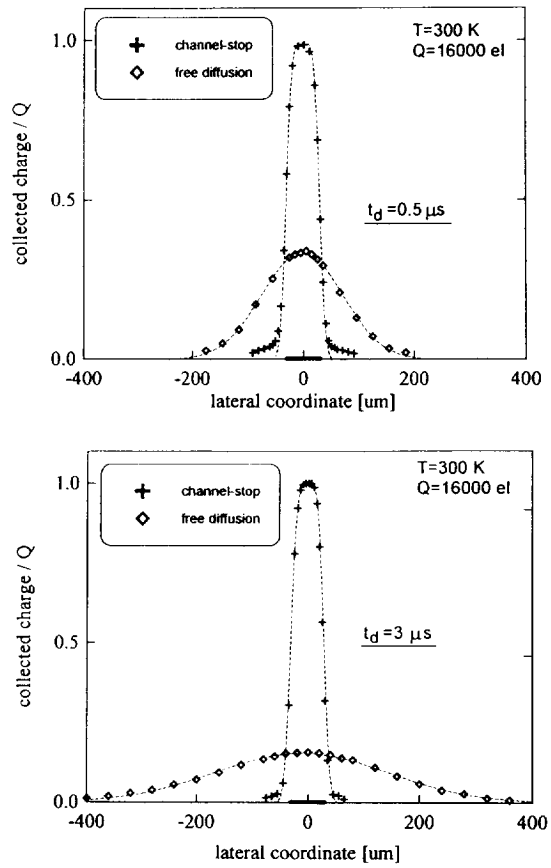

Fig. 7. Measurements of the collected charge at two individual anodes as a function of the lateral position of injection. One anode is in the channel-stop drifting region while the other is in the region where lateral diffusion is free. The dashed lines are least-squares fits obtained from the convolution of a Gaussian (projected electron density along the lateral coordinate) with the rectangular weighting function of one anode. The thicker section on the horizontal axis shows the size of the drift channel, (a) drift time 0.5 μs, (b) drift time 3 μs.

time. When the electrons are confined within the channel-stop implants we assigned the rms width of $P_y/\sqrt{12}$. The theoretical law for pure diffusion $\sigma_{\text{diff}} = \sqrt{2Dt_d}$ is well matched by the experimental points with the room temperature value of the electron diffusion constant (D = 35 cm^2/s). This confirms that for the experimented charge level ($Q \leq 1.6 \times 10^4$ electrons) the electrostatic repulsion between the electrons is negligible [2].

4. Conclusions

We presented the design of a new drift detector aimed at the reduction of the lateral diffusion of electrons by means of an array of deep implants parallel to the drift direction.

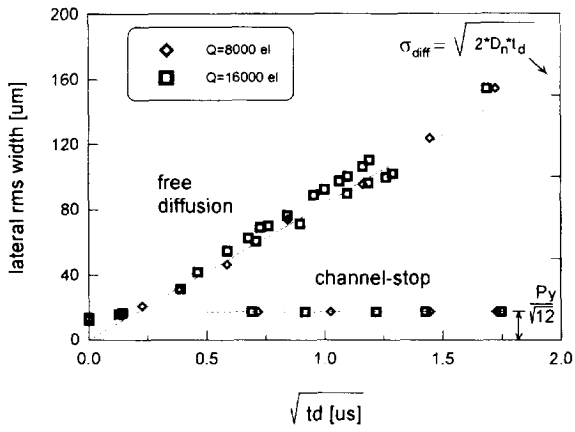

Fig. 8. Lateral rms width of the charge cloud, obtained from the measurements of the collected charge at individual anodes, as a function of the square root of the drift time. When the drift is confined within the channel stop region we assigned the value $P/\sqrt{12}$. The theoretical law for pure diffusion is drawn for $D = 35\,\mathrm{cm}^2/\mathrm{s}$. The experimental points are obtained with two injected charge levels: 8×10^3 and 1.6×10^4 electrons.

First experimental measurements proved the effectiveness of the "channel-stop" implants to confine the electron cloud during the drift. Charge sharing between two adjacent drift channels can be either minimised or made certain by proper design of the initial motion of the signal electrons. In the first case energy resolution comparable with cylindrical SDDs having one central anode can be obtained. In the latter case interpolation of the charge collected at two adjacent anodes can lead to sub-micron resolution in the measurement of the lateral coordinate. Further investigation of the high charge effects is needed in order to complete the picture of the confining mechanism.

As the electrons must travel close to one detector side, surface non-linearity is more important than in "classical" drift detectors. It affects the drift speed and therefore may limit the time resolution. The pitch of the strips on the deep implanted side of the detector must therefore be scaled accordingly to the distance of the electron trajectory from the surface. The minimum value of the strip pitch is practically determined by the constraints posed by the design of an internal voltage divider. Shifting the electron trajectory to a greater distance from the surface achieves a reduction of the drift speed perturbations but also of the lateral potential barrier, although its reduction is slower due to the necessary increase of the thickness of the epitaxial layer. In order to extend the depth of the useful lateral confinement a higher doping of the epitaxial layer and/or higher energy deep p-implants can be chosen according to Eq. (2). Deep n-channels, that form potential wells for the electrons, may also be implanted between the deep p-implants to increase the lateral barrier. A substantial improvement for stabilising the surface conditions is expected covering the oxide layers of the deep implanted side of the detector with metal (field-plate).

Acknowledgements

The authors would like to thank the MPI Halbleiterlabor for the production of the detector. The authors are also grateful to E. Gatti for many fruitful discussions and for the careful reading of the manuscript. A. Castoldi wishes to thank V. Radeka, Instrumentation Division and P. Rehak, Physics Department, for the very kind hospitality at BNL.

This work has been supported by the Italian institution INFN, MURST, CNR and by the U.S. Department of Energy.

This manuscript has been authored under contract number DE-AC02-76CH00016 with the U.S. Department of Energy. Accordingly, the U.S. Government retains a non-exclusive, royalty free licence to publish or reproduce the published form of this contribution, or allow others to do so, for U.S. Government purposes.

References

[1] P. Rehak, et al., Nucl Instr. and Meth. A 248 (1986) 367.
[2] E. Gatti, A. Longoni and M. Sampietro, New developments in solid-state detectors, Solid State Devices, eds. G. Soncini and P.U. Calzolari (Elsevier, North-Holland, 1988).
[3] E. Gatti, A. Longoni, P. Rehak and M. Sampietro, Nucl. Instr. and Meth. A 253 (1987) 393.
[4] H. Bräuninger et al., Nucl. Instr. and Meth. A 326 (1993) 129.
[5] L. Strüder, P. Holl, G. Lutz and G. Kemmer, Nucl. Instr. and Meth. A 257 (1987) 594.
[6] ESA TRP Contract N.8873\90\NL\PB(SC), Final report, Aug. 1991.
[7] G. Baccarani, R. Guerrieri, P. Ciampolini and M. Rudan, HFIELDS: a highly flexible 2-D semiconductor-device analysis program, Nasecode IV, Dublin, Ireland, June 19–21, 1985.
[8] A. Castoldi and P. Rehak, Rev. Sci. Instr. 66(10) (1995) 4989.
[9] A. Longoni, M. Sampietro and L. Strüder, Nucl. Instr. and Meth. A 288 (1990) 35.